Effect of flow oscillations on the liquid film evaporation and instability formation for elongated vapour slugs within heated microchannels.

Manolia Andredaki[1], Anastasios Georgoulas[1*], Nicolas Miche[1] and Marco Marengo[1]

[1]*Advanced Engineering Centre, School of Computing Engineering and Mathematics, University of Brighton, Lewes Road, Brighton BN2 4GJ, East Sussex, UK*

Abstract

An enhanced Volume Of Fluid (VOF) based numerical simulation framework that accounts for conjugate heat transfer between a solid region and a two-phase flow region with phase-change due to evaporation and/or condensation, is applied in order to investigate the effect of global flow oscillation frequency and amplitude on the liquid film evaporation and instability formation, around isolated, elongated vapour slugs, within a heated micro-channel, in saturated flow boiling conditions. A series of numerical simulations are performed, for different values of flow oscillation amplitude and frequency. The oscillations are induced by applying an oscillating pressure boundary condition at the inlet of the channel, keeping the pressure constant at the outlet, after an initial period of constant pressure drop between the inlet and the outlet of the channel. R245fa, FC72 and Ethanol are used as the working fluids. Capillary ridges that are initiated at the liquid film, in the vicinity of the leading edge of the considered vapour slug, are identified as a result of the imposed oscillations. It is shown that the generation frequency as well as the height of the proposed ridges, are directly related to the corresponding frequency and amplitude of the induced flow oscillations. Furthermore, comparing the vapour volume increase with respect to time for different oscillation frequencies and amplitudes, it is shown that the liquid film evaporation is enhanced with the increase of the oscillation amplitude while it degrades as the frequency of the oscillation becomes higher.

Keywords: Volume of Fluid, Conjugate Heat Transfer, Oscillating Vapour Slug, Micro-channel

1. INTRODUCTION

The demand for increasingly higher performances of electronic equipment, has pushed researchers and engineers to develop a new generation of heat dissipation systems based on the local phase-change of a working fluid. Efficient thermal control, of densely packed electronic components, has become of crucial importance. Flow boiling within micro-channels, constitute one of the most promising cooling technologies to dissipate high heat fluxes from micro-scale electronic components (e.g. micro-processors). Two-phase cooling devices utilising evaporators consisting of micro-channels that are in direct contact with a micro-chip, can remove heat fluxes up to 300 W/cm^2 [1]. However, the flow complexity in cases of multi-microchannel two-phase flow evaporators, can lead to high-amplitude and high-frequency temperature and pressure oscillations [2]. Such oscillations, in the slug flow regime, may generate significant instabilities in the liquid film that surrounds elongated vapour slugs. Such flow oscillations and instabilities are also present in the case of oscillating, closed loop, two-phase cooling devices, such as Pulsating Heat Pipes that might consist of micro- (e.g. [3]) or mini-channels (e.g. [4]).

In the present paper, an enhanced Volume Of Fluid (VOF) based numerical simulation framework that accounts for conjugate heat transfer between a solid region and a two-phase flow region with phase-change due to evaporation and/or condensation, is applied in order to investigate the effect of global flow oscillation frequency and amplitude on the liquid film evaporation and instability formation, around isolated, elongated vapour slugs, within a heated micro-channel, in saturated flow boiling conditions.

2. INVESTIGATION METHODOLOGY

2.1 Numerical Method

2.1.1 Governing Equations

In this section, the governing equations for mass, momentum, energy, and volume fraction are presented. It should be mentioned that liquid and vapour phases are both treated as incompressible, Newtonian fluids. The mass conservation equation is given as:

$$\nabla \cdot \left(\rho \vec{U}\right) = \dot{\rho} \tag{1}$$

where U is the fluid velocity and ρ is the bulk density. The source term on the right-hand side accounts for the phase change. The conservation of momentum is given by the following equation:

$$\frac{\partial}{\partial t}\left(\rho \vec{U}\right) + \nabla \cdot \left(\rho \vec{U}\vec{U}\right) - \nabla \cdot \left\{\mu \left[\nabla \vec{U} + \left(\nabla \vec{U}\right)^{T}\right]\right\} = -\nabla p + \vec{f}_{ST} + \vec{f}_{g} \tag{2}$$

where p is the pressure and μ is the bulk dynamic viscosity. The momentum source terms in the right-hand side of the equation account for the effects of surface tension and gravity, respectively. The surface tension term is modelled according to the classical approach of Brackbill et al. [5]. The conservation of energy balance is given by the following equation:

$$\frac{\partial}{\partial t}(\rho c_p T) + \nabla \cdot (\vec{U}\rho c_p T) - \nabla \cdot (\lambda \nabla T) = \dot{h} \qquad (3)$$

where c_p is the bulk heat capacity, T the temperature field, and λ is the bulk thermal conductivity. The source term on the right-hand side of the equation represents the contribution of the enthalpy of evaporation/condensation or else the cooling/heating associated with the latent heat of the phase-change. The volume fraction α is advected by the flow field by the following equation:

$$\frac{\partial \alpha}{\partial t} + \nabla \cdot (\alpha \vec{U}) - \nabla \cdot (\alpha(1-\alpha)U_r) = \frac{\dot{\rho}}{\rho}\alpha \qquad (4)$$

Interface sharpening is very important in simulating two-phase flows of two immiscible fluids. In OpenFOAM the sharpening of the interface is achieved artificially by introducing the extra compression term $\nabla \cdot (\alpha(1-\alpha)U_r)$ in Equation (4). Ur is an artificial compression velocity. The divergence of the compression velocity U_r, ensures the conservation of the volume fraction α, while the term α(1-α) limits this artificial compression approach only in the vicinity of the interface, where $0 < \alpha < 1$ [6]. The level of compression depends on the value of C_γ ([6], [7]). For the simulations of the present investigation, initial, trial simulations indicated that a value of Cγ =1 should be used, in order to maintain a quite sharp interface without at the same time having unphysical results. The source term on the right-hand side of the Equation (4) is needed because, due to the local mass source terms, the velocity field is not free of divergence. Finally, the bulk fluid properties γ are computed as the averages over the liquid (γ_l) and vapour (γ_v) phases, weighted with the volume fraction α. The VOF-based solver that is used in the present investigation has been modified accordingly in order to account for an adequate level of spurious currents suppression. More details on the proposed validation as well as on the proposed improved VOF method can be found in the paper by Georgoulas et al [8].

The conservation of energy equation in the solid domains is defined as:

$$\frac{\partial}{\partial t}(\rho_s c_{ps} T) = \nabla \cdot (\lambda_s \nabla T) \qquad (5)$$

The coupling at the boundary between the solid region and fluid region is achieved iteratively through the following boundary condition:

$$T_f = T_s \qquad (6)$$

$$\lambda_f \frac{\partial T_f}{\partial n} = \lambda_s \frac{\partial T_s}{\partial n} \qquad (7)$$

2.1.2 Phase Change Model

The utilized phase change model that was implemented in the improved OpenFOAM VOF solver that is used in the present investigation, will be described briefly in this section. Supplementary details can be found in the work by Georgoulas et al. [9]. In the case of evaporation, the evaporating mass flux at the liquid - vapour interface j_{evap} is calculated from the following equation:

$$j_{evap} = \frac{T_{int} - T_{sat}}{R_{int} h_{lv}} \qquad (8)$$

where T_{int} is the temperature of the interface, T_{sat} is the saturation temperature, R_{int} is the interfacial heat resistance and h_{lv} is the latent heat of evaporation at the saturation temperature. The amount of liquid that evaporates is calculated locally and the resulting source term field is smeared over a few cells in order to avoid numerical instabilities. The evaporating mass is taken away on the liquid side of the interface and reappears on the vapour side, following the process suggested in the work of Hardt and Wondra [10]. Further details on the proposed process can be found in the work of Georgoulas et al. [9].

2.1 Validation of Numerical Framework

The utilised, enhanced, VOF-based numerical model, has been extensively validated in the past against existing analytical solutions and experimental data on adiabatic and diabatic bubble and droplet dynamics [8], [9], [11], [12]. Some, of these validation results are reproduced in the following figures.

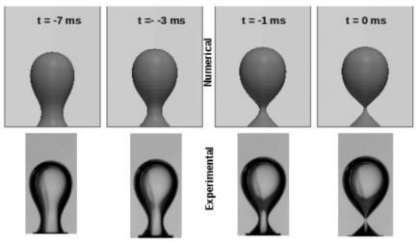

Figure 1. Comparison of experimental and numerical results, for the case of adiabatic, quasi-static bubble growth and detachment from a submerged orifice into an isothermal liquid pool [8].

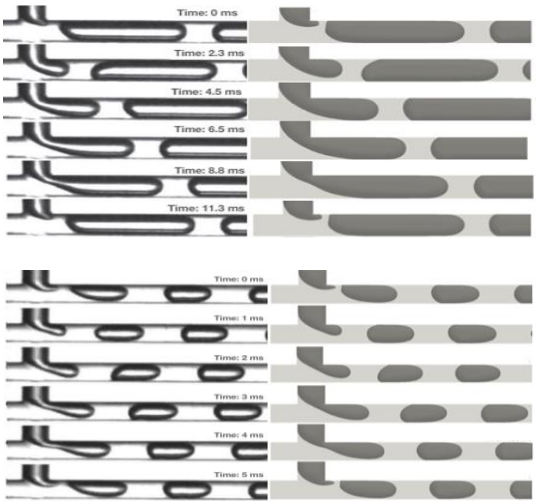

Fig. 2. Comparison of experimental (left) and numerical results, for the three different cases of Taylor bubble generation in a T-junction [12].

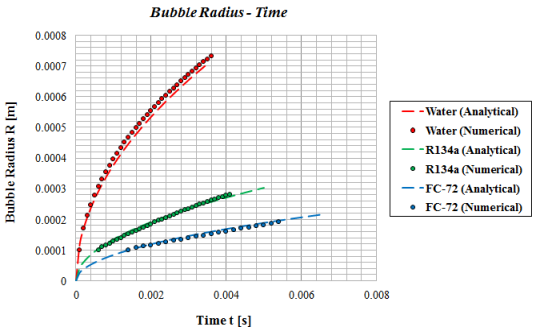

Figure 3. Comparison between numerical simulation and analytical solution results, for a vapour bubble growing in an infinite superheated liquid domain [9].

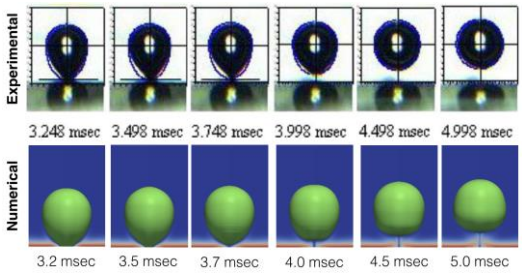

Figure 4. Comparison of experimental and numerical results, for the case of bubble growth and detachment from a superheated plate (saturated pool boiling) [9].

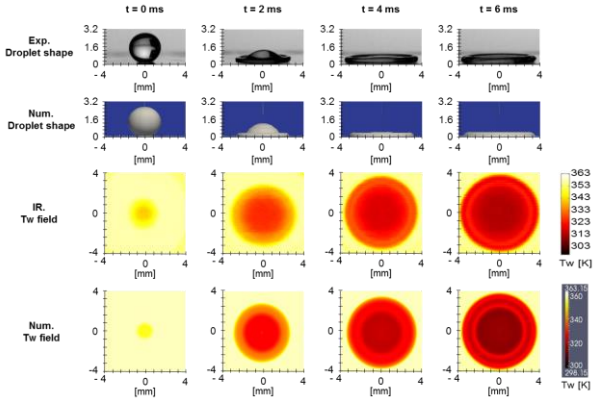

Figure 5. Comparison between high-speed recorded and numerically predicted droplet shape and between experimentally measured and numerically calculated temperature field (Tw) at the bottom of the solid sample, during droplet impact cooling [11].

As it can be observed the proposed VOF-based numerical modelling framework, accurately predicts adiabatic and diabatic bubble and droplet dynamics as well as conjugate heat transfer between solid and fluid domains. Therefore, it can safely be used for the purposes of the present investigation.

3. APPLICATION OF THE VALIDATED NUMERICAL METHOD

3.1 Numerical Simulation Set-up

In the current section of the present work the previously described, VOF-based, numerical simulation framework is further applied for the conduction of parametric numerical simulations, aiming to identify and quantify the effect of global flow oscillation frequency and amplitude on the liquid film evaporation and instability formation, around isolated, elongated vapour slugs, within a heated micro-channel, in saturated flow boiling conditions.

In more detail, a series of numerical experiments, for a specific value of applied heat flux ($q=5{,}000 W/m^2$) in the heated section of the considered circular micro-channel (Do = 0.69 mm, Di=0.5 mm) and for different values of oscillation amplitude and frequency, is conducted. The flow oscillations were generated inducing an oscillating pressure boundary condition at the inlet of the channel while keeping the pressure constant at the outlet. The same parametric analysis is carried out for three different working fluids: R245fa, FC72 and Ethanol. Each simulation is conducted in three stages. At the first stage a single-phase simulation is run with only liquid flowing into the channel, applying a constant pressure drop of ΔP = 500 Pa

and a constant heat flux of q= 5,000 W/m^2 at the heated part of the considered micro-channel. In the second stage, after the single-phase flow has reached a steady state and the hydrodynamic and thermal boundary layers have been developed (t=0.2 s), an elongated vapour slug is patched upstream of the heated section of the microchannel at a certain distance from the channel inlet, having an initial length of 3xDi and an initial liquid film thickness of $h_{film(init)}$ = 20μm. This initial vapor slug is then left to be carried away downstream by the previously developed liquid flow, towards the heated section of the circular micro-channel. At the third and final stage, after 0.018 s that the vapour slug front has reached approximately the middle of the channel in each case (ensuring that it is completely contained within the heated region), an oscillating relative pressure boundary condition is imposed at the inlet of the channel, keeping the relative pressure at the outlet constant at 0 Pa. The resulting pressure value for the inlet with respect to time, can be described by the following equation.

$$P(t) = (1 + \alpha \sin(\pi f t))P_{ref} + P_0 \quad (9)$$

where α and f are the amplitude and frequency of the oscillation, while P_0 and P_{ref} are the initial pressure and a reference pressure, respectively. An axisymmetric computational domain is constructed with the axis of symmetry coinciding with the central/longitudinal axis of the considered circular micro-channel. The computational domain, mesh and the applied boundary conditions as well as the initial condition for the oscillating part of the simulations, are illustrated in Fig. 6.

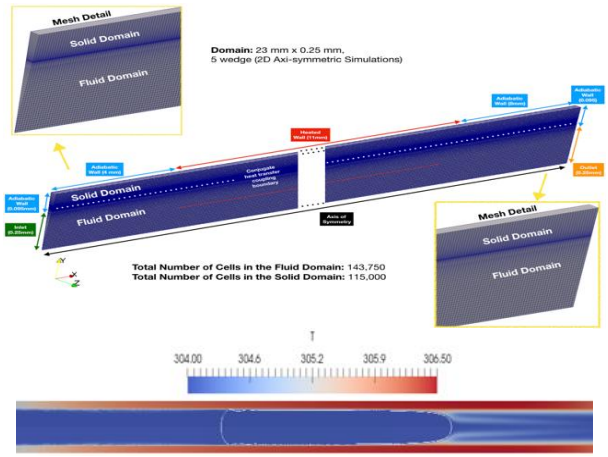

Figure 6. Geometry, Mesh and Boundary conditions (top), initial state before imposed flow oscillations (bottom).

The computational domain consists of a solid and a fluid region that are coupled at their interface. The fluid and solid domains consist of a total number of 143,750 and 115,00 computational cells, respectively. The mesh density was selected after a mesh independency study. A structured mesh, consisting of hexahedral and prismatic elements is used, with a grid clustering towards the coupling interface between the solid and fluid regions. The overall computation domain constitutes a 5^0 wedge of the circular micro-channel under consideration, since this is the way that 2D axisymmetric simulations are conducted in OpenFOAM, the open-source CFD platform that is utilized for the overall computations.

Table 1, summarizes the imposed oscillation characteristics and the working fluid, for each of the examined cases, in the present numerical investigation.

Table 1. Inlet pressure oscillation characteristics and working fluid for the considered cases.

Case	Pressure Oscillation Amplitude [Pa]	Pressure Oscillation Frequency [Hz]	Working Fluid
1	100,000	500	R245fa
2	100,000	750	R245fa
3	100,000	1000	R245fa
4	50,000	500	R245fa
5	75,000	500	R245fa
6	100,000	500	FC72
7	100,000	750	FC72
8	100,000	1000	FC72
9	50,000	500	FC72
10	75,000	500	FC72
11	100,000	500	Ethanol
12	100,000	750	Ethanol
13	100,000	1000	Ethanol
14	50,000	500	Ethanol
15	75,000	500	Ethanol

3.2 Effect of Flow Oscillation Frequency

The spatial and temporal evolution of the considered vapour slugs, under different pressure oscillation frequencies at the inlet of the considered micro-channel, is depicted in Figures 7, 8 and 9 were the numerical simulation results for cases 1-3 (R245fa), 6-8 (FC72) and 11-13 (Ethanol) from Table 1 are presented, respectively (induced flow oscillation frequency increase). As it can be observed in all 9 cases, apart from the capillary waves that are present in the trailing edge of the slug at the beginning of the oscillation period (formed during the constant pressure drop stage), the imposed flow oscillations are responsible for the periodic generation of a capillary ridge in the

vicinity of the leading edge of the evaporating vapour slug, that is then traveling downstream towards its trailing edge, gradually attenuating, reducing its maximum height and increasing its overall length. It is worth noticing that in all 9 cases the period of the capillary ridge generation, coincides with the period of a complete pressure oscillation at the inlet of the considered microchannel (i.e. every 2 ms for cases 1, 6 and 11, every 1.33 ms for cases 2, 7 and 12 and every 1 ms, for cases 3, 8 and 13). It is also evident that for all three working fluids considered, the increase in the pressure oscillation frequency at the inlet of the considered micro-channel, is accompanied by a reduction in the maximum height of the periodically generated capillary ridge, in each case. Some interesting inertial phenomena are also evident in all nine cases, that result in the encapsulation of small liquid droplets within the elongated vapour bubble and/or in the detachment of small satellite bubbles from its leading and/or its trailing edge. The proposed phenomena are enhanced with the oscillation frequency increase. Finally, it should be noticed that in the case of Ethanol the generated capillary ridges are not very intense, as in the other two fluids, due to the higher surface tension coefficient.

In order to quantify the effect of the flow oscillation frequency, in the evaporation of the liquid film between the elongating vapour slug and the heated wall of the channel, the vapour slug volume increase with time is plotted for each of the considered working fluids in Figure 10. As it can be observed, for all three simulated working fluids, the increase in flow oscillation frequency causes a significant decrease in the liquid film evaporation. The proposed effect progressively increases with time. In the case of Ethanol and for flow oscillation frequency of 500 Hz, just after t=3ms, a decrease in the vapour volume is observed for a small time period of approximately 0.4 ms. This can be attributed to the significant amount of liquid that has been encapsulated in the form of droplets within the elongating vapour slug in this case (please see Case 11 in Figure 9).

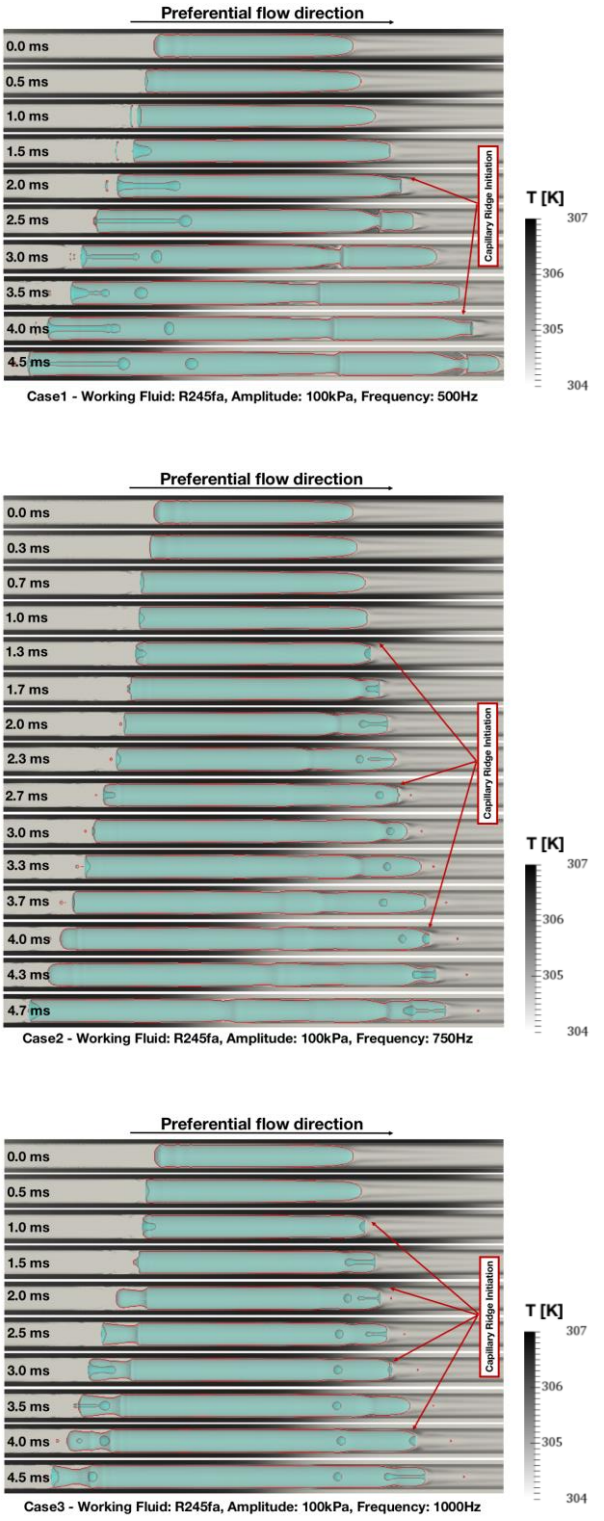

Figure 7: Spatial and temporal evolution of vapour slug after the initiation of the oscillating pressure boundary condition at the inlet. Case 1, case 2 and case 3, from Table 1. The camera view is moving along with the vapour slug, as it progresses downstream within the considered micro-channel (effect of flow oscillation frequency-R245fa).

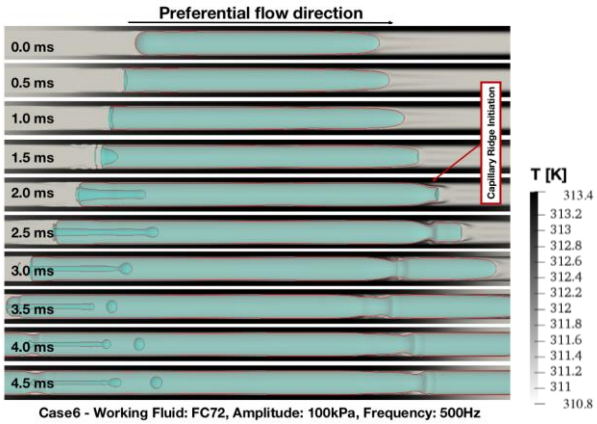

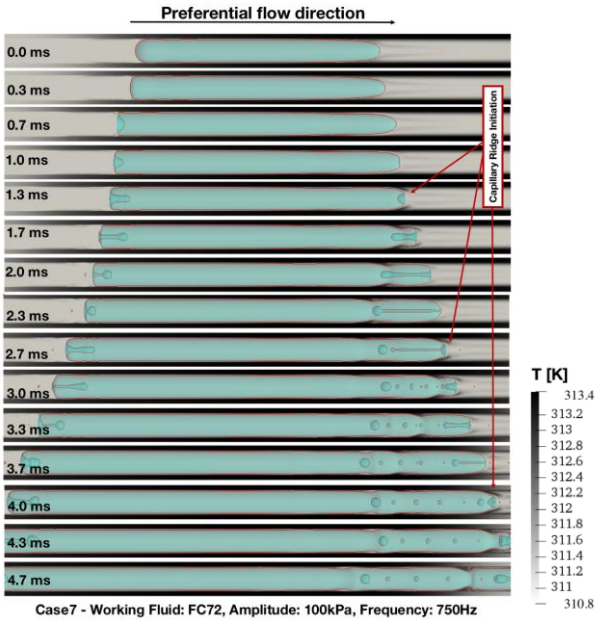

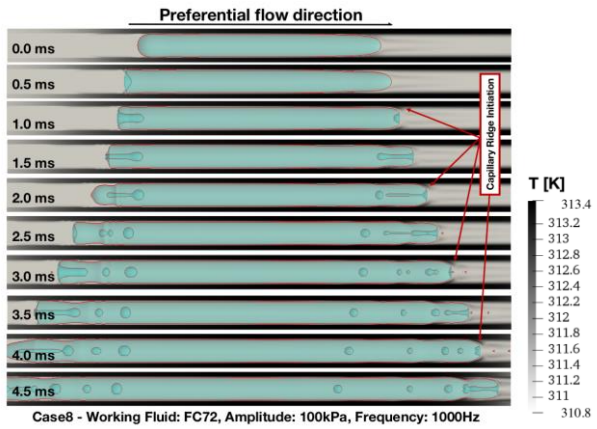

Figure 8: Spatial and temporal evolution of vapour slug after the initiation of the oscillating pressure boundary condition at the inlet. Case 6, case 7 and case 8, from Table 1. The camera view is moving along with the vapour slug, as it progresses downstream within the considered micro-channel (effect of flow oscillation frequency-FC72).

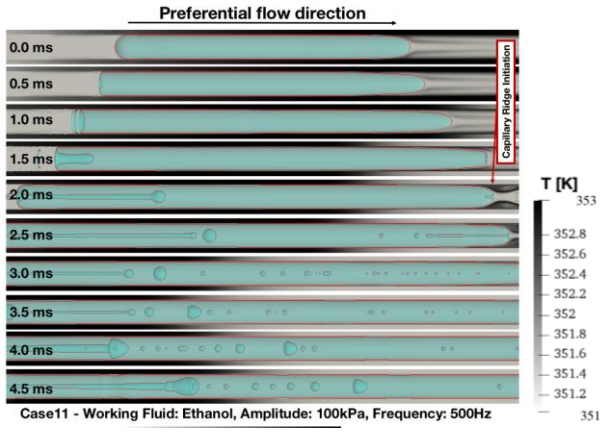

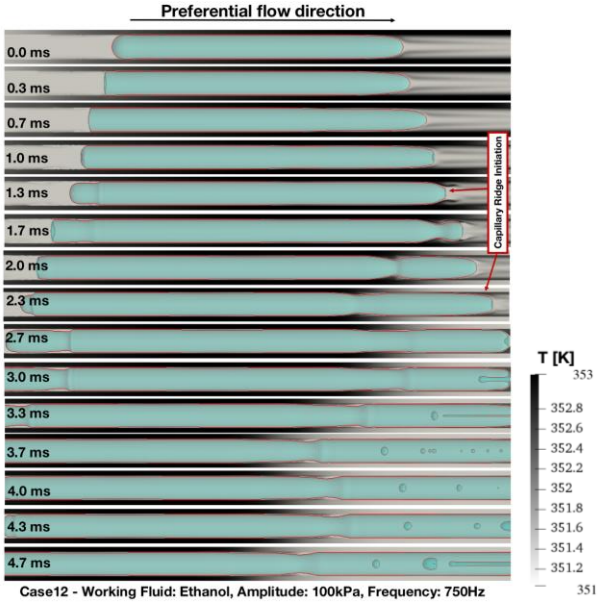

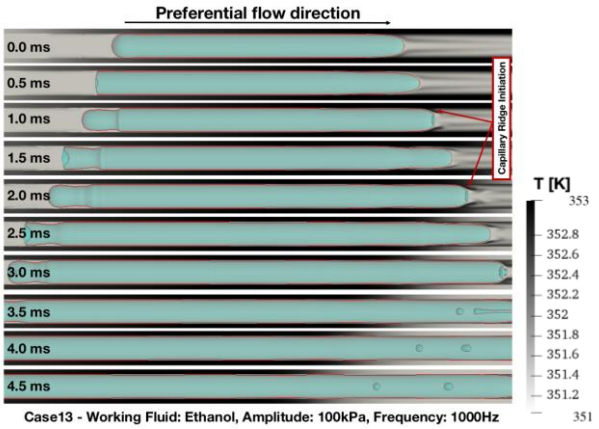

Figure 9: Spatial and temporal evolution of vapour slug after the initiation of the oscillating pressure boundary condition at the inlet. Case 11, case 12 and case 13, from Table 1. The camera view is moving along with the vapour slug, as it progresses downstream within the considered micro-channel (effect of flow oscillation frequency-Ethanol).

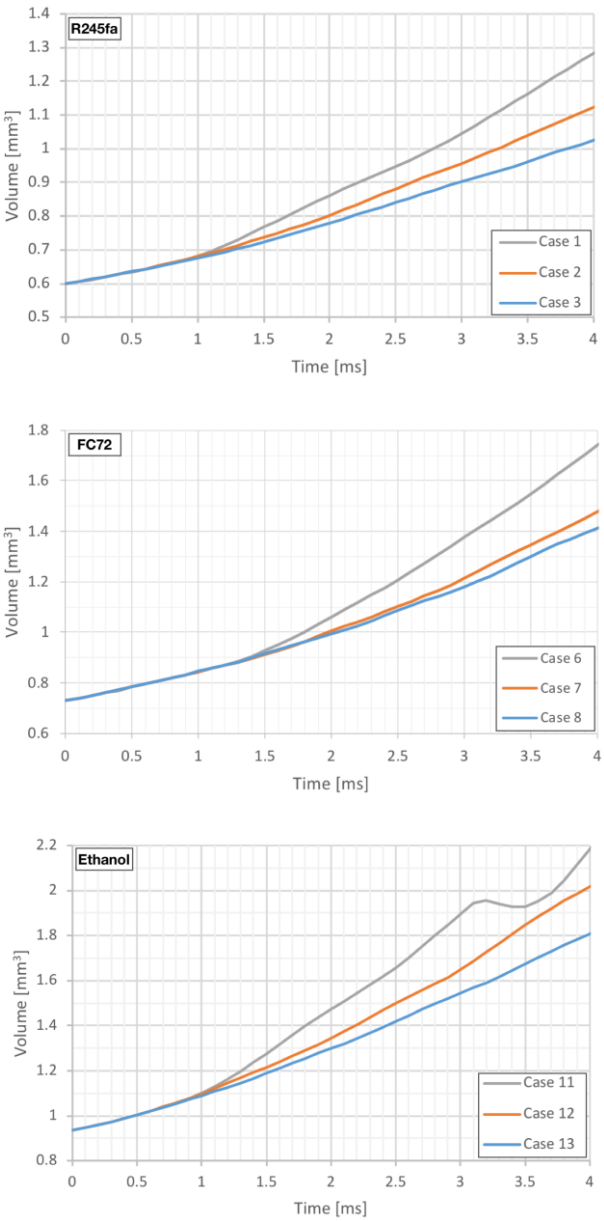

Figure 10: Vapour slug volume with respect to time, from the beginning of the imposed oscillation (Effect of flow oscillation frequency in the liquid film evaporation).

3.3 Effect of Flow Oscillation Amplitude

The spatial and temporal evolution of the considered vapour slugs, under different pressure oscillation amplitudes at the inlet of the considered micro-channel, is depicted in Figures 10, 11 and 12 were the numerical simulation results for i) cases 5, 4 and 1 (R245fa), ii) cases 9, 10 and 6 (FC72), and iii) 14, 15 and 11 (Ethanol), from Table 1 are presented, respectively (induced flow oscillation amplitude increase).

As it can be observed in these cases, for all three of the considered working fluids, the increase of the flow oscillation amplitude, causes a corresponding increase in the maximum height of the periodically developed capillary ridges in the vicinity of the leading edge of the evaporating vapour slug.

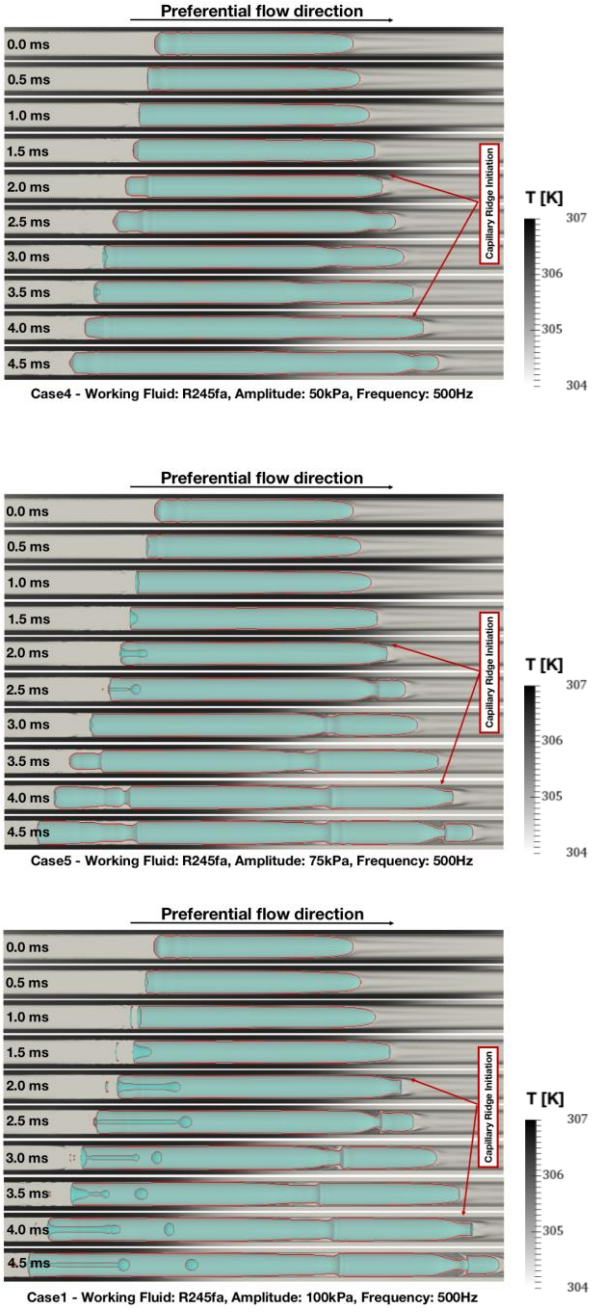

Figure 11: Spatial and temporal evolution of vapour slug after the initiation of the oscillating pressure boundary condition at the inlet. Case 4, case 5 and case 1, from Table 1. The camera view is moving along with the vapour slug, as it progresses downstream within the considered micro-channel (effect of flow oscillation amplitude-R245fa).

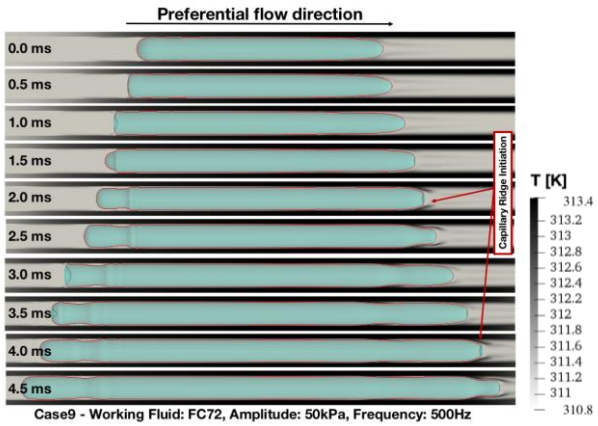

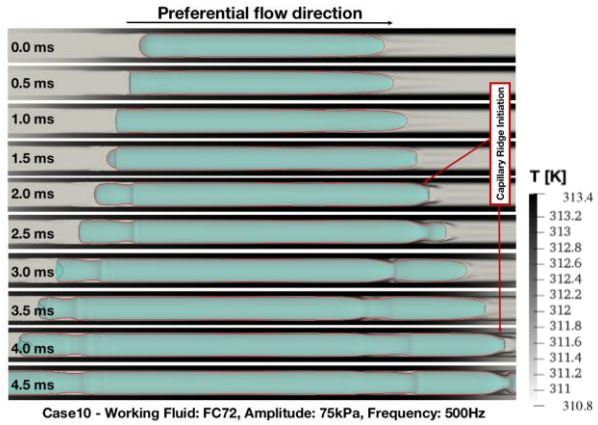

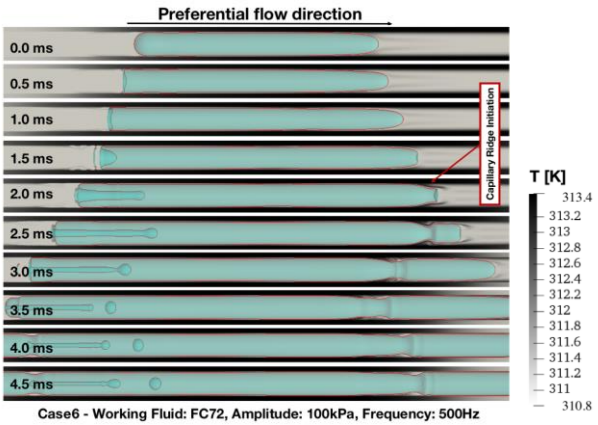

Figure 12: Spatial and temporal evolution of vapour slug after the initiation of the oscillating pressure boundary condition at the inlet. Case 9, case 10 and case 6, from Table 1. The camera view is moving along with the vapour slug, as it progresses downstream within the considered micro-channel (effect of flow oscillation amplitude-FC72).

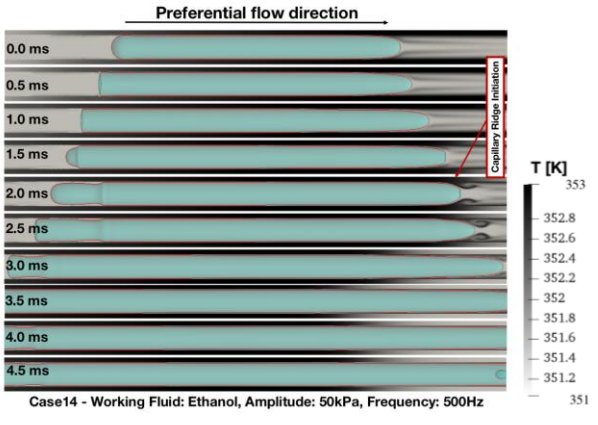

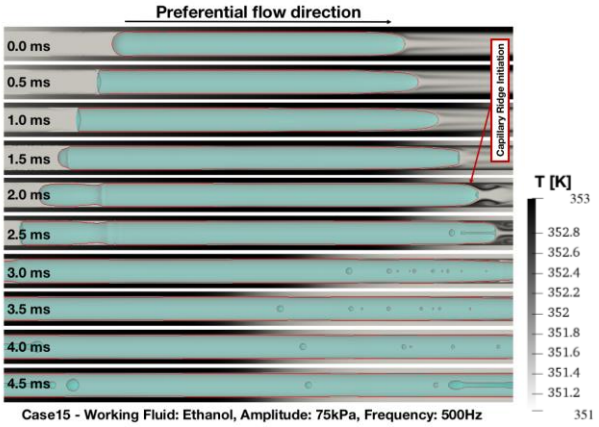

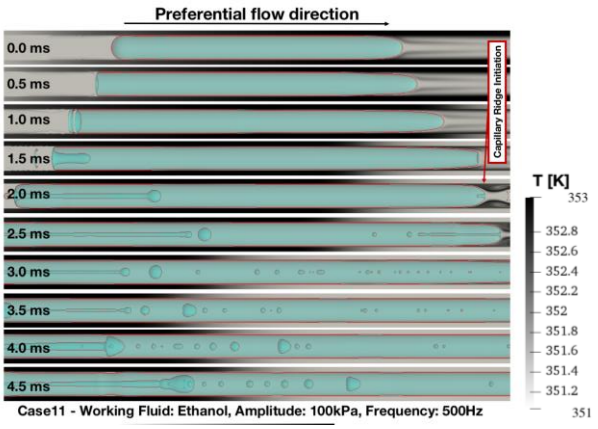

Figure 13: Spatial and temporal evolution of vapour slug after the initiation of the oscillating pressure boundary condition at the inlet. Case 14, case 15 and case 11, from Table 1. The camera view is moving along with the vapour slug, as it progresses downstream within the considered micro-channel (effect of flow oscillation amplitude-Ethanol).

In order to quantify the effect of the flow oscillation amplitude, in the evaporation of the liquid film between the elongating vapour slug and the heated wall of the channel, the vapour slug volume increase with time is again plotted for each of the considered working fluids in Figure 14. As it can be observed for all three simulated working fluids, the increase in flow oscillation amplitude causes a significant increase in the liquid film evaporation. The proposed effect progressively increases with time.

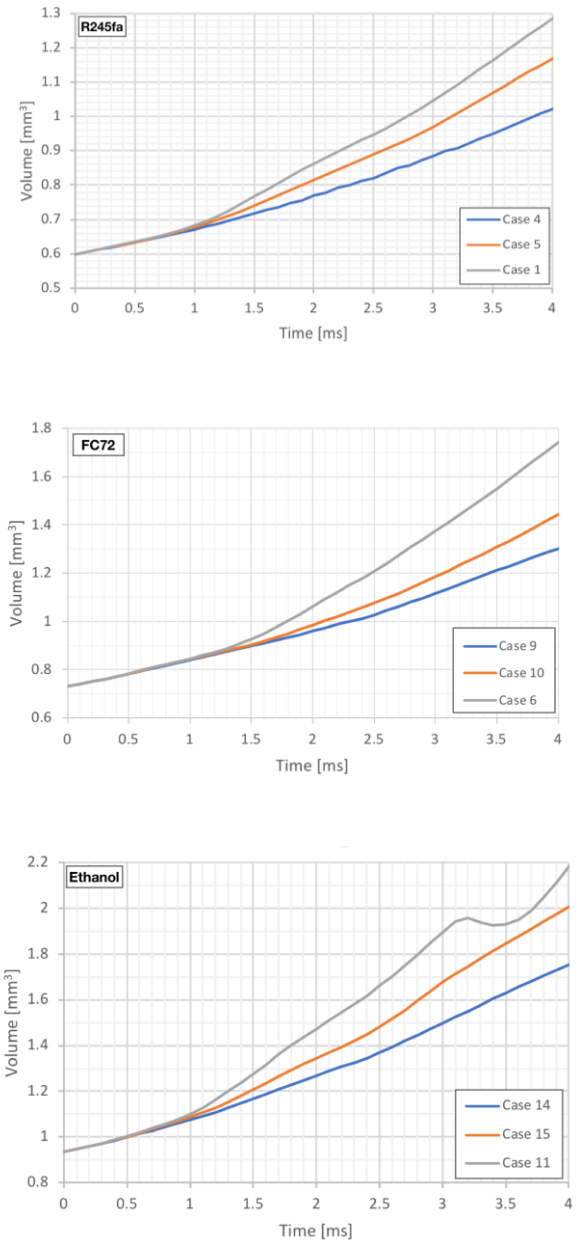

Figure 14: Vapour slug volume with respect to time, from the beginning of the imposed oscillation (Effect of flow oscillation amplitude in the liquid film evaporation).

4. CONCLUSION

In the present paper, a previously validated and optimized, enhanced, VOF-based numerical modelling framework is applied in order to identify and quantify the effects of global flow oscillation frequency and amplitude on the liquid film evaporation and instabilities formation, around isolated, elongated vapour slugs, within a heated micro-channel, in saturated flow boiling conditions. Three different working fluids are simulated for three different flow oscillation frequencies and amplitudes, in each case.

From the post-processing and analysis of the results it is obvious that after the application of the induced flow oscillation, capillary ridges are periodically formed in the liquid film between the vapour slug and the heated wall of the channel, in the vicinity of the trailing edge of the elongating bubble, as it moves towards the outlet. It is shown for the first time that the period of formation coincides with the period of the induced flow oscillations. This is evident for all three of the simulated working fluids.

Another important conclusion is that for all three working fluids considered, the increase in the flow oscillation frequency, is accompanied by a reduction in the maximum height of the periodically generated capillary ridges, while the increase in the flow oscillation amplitude, causes a corresponding increase in their maximum height.

Finally, the liquid film evaporation rate is significantly enhanced by the corresponding increase of the flow oscillation amplitude, while it is diminished by the increase of the flow oscillation frequency.

The overall findings of the present numerical investigation add significant insight into the effect and importance of flow oscillations in the hydrodynamic and phase-change characteristics of slug plug flows within micro-channels that are of interest to multi-microchannel two-phase flow evaporators as well as to oscillating, closed loop, two-phase cooling devices, such as Pulsating Heat Pipes.

For future investigations the content of the present paper can be further extended by performing similar parametric numerical investigations also for the case of mini-channels.

ACKNOWLEDGEMENT

The Authors would like to acknowledge UK's Engineering and Physical Science Research Council support, through the grant EP/P013112/1.

REFERENCES

[1] M. Magnini, B. Pulvirenti, and J. R. Thome, "Numerical investigation of hydrodynamics and heat transfer of elongated bubbles during flow boiling in a microchannel," *Int. J. Heat Mass Transf.*, vol. 59, pp. 451–471, Apr. 2013.

[2] S. Szczukiewicz, M. Magnini, and J. R. Thome, "Proposed models, ongoing experiments, and latest numerical simulations of microchannel two-phase flow boiling," *Int. J. Multiph. Flow*, vol. 59, pp. 84–101, Feb. 2014.

[3] J. Lee and S. J. Kim, "Effect of channel geometry on the operating limit of micro pulsating heat pipes," *Int. J. Heat Mass Transf.*, vol. 107, pp. 204–212, Apr. 2017.

[4] D. Mangini, M. Mameli, A. Georgoulas, L. Araneo, S. Filippeschi, and M. Marengo, "A pulsating heat pipe for space applications: Ground and microgravity experiments," *Int. J. Therm. Sci.*, vol. 95, 2015.

[5] J. . Brackbill, D. . Kothe, and C. Zemach, "A continuum method for modeling surface tension," *J. Comput. Phys.*, vol. 100, no. 2, pp. 335–354, Jun. 1992.

[6] D. A. Hoang, V. van Steijn, L. M. Portela, M. T. Kreutzer, and C. R. Kleijn, "Benchmark numerical simulations of segmented two-phase flows in microchannels using the Volume of Fluid method," *Comput. Fluids*, vol. 86, pp. 28–36, Nov. 2013.

[7] S. S. Deshpande, L. Anumolu, and M. F. Trujillo, "Evaluating the performance of the two-phase flow solver interFoam," *Comput. Sci. Discov.*, vol. 5, no. 1, p. 14016, 2012.

[8] A. Georgoulas, P. Koukouvinis, M. Gavaises, and M. Marengo, "Numerical investigation of quasi-static bubble growth and detachment from submerged orifices in isothermal liquid pools: The effect of varying fluid properties and gravity levels," *Int. J. Multiph. Flow*, vol. 74, pp. 59–78, 2015.

[9] A. Georgoulas, M. Andredaki, and M. Marengo, "An enhanced VOF method coupled with heat transfer and phase change to characterise bubble detachment in saturated pool boiling," *Energies*, vol. 10, no. 3, 2017.

[10] S. Hardt and F. Wondra, "Evaporation model for interfacial flows based on a continuum-field representation of the source terms," *J. Comput. Phys.*, vol. 227, no. 11, pp. 5871–5895, 2008.

[11] E. Teodori, P. Pontes, A. Moita, A. Georgoulas, M. Marengo, and A. Moreira, "Sensible heat transfer during droplet cooling: Experimental and numerical analysis," *Energies*, vol. 10, no. 6, 2017.

[12] M. Andredaki, A. Georgoulas, N. Miché, and M. Marengo, "Break-up Mechanisms and Conditions for Vapour Slugs Within Mini-Channels," in *15th UK Heat Transfer Conference, UKHTC2017, Brunel University London, 4-5 September 2017*, 2017.